

Diffractive elastic scattering and hadronic radii: Geometric and Pomeron approaches

J. Hüfner and B. Povh

Institut für Theoretische Physik der Universität Heidelberg and Max-Planck-Institut für Kernphysik, P.O. Box 103980, 6900 Heidelberg, Germany

(Received 23 October 1991; revised manuscript received 6 April 1992)

A parametrization based on geometric concepts is proposed for the spin-independent part of the amplitude $A_{12}(s,t)$ for elastic scattering of hadrons 1 and 2 at center-of-mass energies $\sqrt{s} \gtrsim 20$ GeV. The dependence on the squared momentum transfer t is described by the form factors $F_i(t, R_i^2(s))$ for each hadron and contain energy-dependent complex radii $R_i(s)$. Data on differential cross sections for pp , $p\bar{p}$, and πp as well as the energy dependence of the total cross section and the slope parameter are reproduced with few adjustable parameters. When our parametrization for $A_{12}(s,t)$ is compared to the one from the Pomeron approach strong similarities emerge.

PACS number(s): 13.85.Dz, 12.40.Pp, 13.40.Fn, 13.85.Lg

I. INTRODUCTION

The understanding of elastic hadron-hadron scattering is an iterative process within a triangle formed by experiment, theory, and phenomenology, the driving force being the data. New experiments mostly at higher energies led to refinements or even revisions of earlier descriptions. In this paper we restrict ourselves to the energy regime $\sqrt{s} \gtrsim 20$ GeV, where elastic scattering is called "diffractive." The data mainly come from experiments performed at the CERN ISR, CERN SPS, and Fermilab accelerators. As an introduction to the present status in the field, we gave in Ref. [1] several reviews and conference proceedings. The theoretical concepts are Pomeron exchange [2] and gluonic interactions [3]; the relation between both approaches is still being worked on [4]. Expressions for cross sections based on either theory contain adjustable parameters. The phenomenological approaches [5–7] are mostly based on geometric concepts; i.e., the size and shape of the colliding objects determine the total and differential cross sections.

Within the triangle of data, theory, and phenomenology, we present a refined phenomenological approach based on geometric concepts. Its free parameters are mostly related to effective energy-dependent complex radii. By comparing the amplitude in our geometric approach with the amplitude in the Pomeron parametrization, we are able to reduce the number of free parameters in each of the approaches. In particular, we are able to derive an expression for the slope of the Pomeron trajectory. We present our approach in Sec. II, show the comparison with experiment in Sec. III, and relate it in Sec. IV to the Pomeron picture.

II. GENERAL EXPRESSION FOR THE SCATTERING AMPLITUDE

We denote by $A_{12}(s,t)$ the spin-independent part of the amplitude for elastic scattering of two hadrons 1 and 2 as a function of the squared c.m. energy s and squared momentum transfer t . The differential and total cross

sections derived from $A_{12}(s,t)$ (spin being neglected) are

$$\frac{d\sigma_{12}^{\text{el}}}{d|t|}(s,t) = \frac{\pi}{s^2} |A_{12}(s,t)|^2, \quad (2.1)$$

$$\sigma_{12}^{\text{tot}}(s) = \frac{4\pi}{s} \text{Im} A_{12}(s,0). \quad (2.2)$$

Frequently, we will also refer to the slope parameter at $t=0$ defined by

$$b_{12}(s) = \frac{d}{dt} \ln \frac{d\sigma_{12}^{\text{el}}}{d|t|}(s,t) \Big|_{t=0}. \quad (2.3)$$

Our phenomenological approach for the amplitude $A_{12}(s,t)$ rests on two experimental observations: the relation between the shape of the differential cross section and hadronic form factors (Chou-Yang observation [5]) and a relation between total cross sections and slope parameters. We find a parametrization which incorporates both relations and which is then generalized in order to incorporate the requirements of analyticity.

A. Chou-Yang observation

When analyzing the differential cross sections for high-energy pp collisions available at that time, Chou and Yang [5] observed that the t dependence of the differential elastic cross section is closely related to the charge form factors $F_i(t)$ $i=1,2$ of the colliding hadrons. Their observation may be written as

$$A_{12}(s,t) \propto F_1(t)F_2(t). \quad (2.4)$$

For small values of t the form factors are related to the mean-squared charge radii $\langle r^2 \rangle_i$ via

$$F_i(t) = 1 + \frac{1}{6} \langle r_{\text{ch}}^2 \rangle_i t + \mathcal{O}(t^2), \quad (2.5)$$

which relation implies that the slope parameter b_{12} is related to the charge radii via

$$b_{12} = \frac{1}{3} (\langle r_{\text{ch}}^2 \rangle_1 + \langle r_{\text{ch}}^2 \rangle_2). \quad (2.6)$$

Although Eqs. (2.4)–(2.6) hold for any shape of $F_i(t)$, we

will rely on a specific functional dependence of $F_i(t)$, which makes generalizations to complex energy-dependent radii particularly easy. We will assume

$$F_i(t) = (1 - t/\Lambda_i^2)^{-n_i}, \quad (2.7)$$

where experiment (and quark-counting rules) suggests $n_i=1$ for mesons and $n_i=2$ for baryons. The only parameter Λ_i is then directly related to the radius via

$$\langle r_{\text{ch}}^2 \rangle_i = \frac{6n_i}{\Lambda_i^2}. \quad (2.8)$$

The particular shape [Eq. (2.7)] for the *hadronic* form factor $F_i(t)$ is rather arbitrary. In the notation of electromagnetic form factors, Eq. (2.7) corresponds to $G_E^i(t)$, but we retain only the functional form of $G_E^i(t)$ and consider Λ_i a free parameter. This approach differs from the one by Donnachie and Landshoff [2], who postulate that the Pomeron couples to the nucleon like a photon. Then their hadronic form factors are identical to the electromagnetic ones.

B. Systematics σ_{12}^{tot} versus b_{12}

In previous papers [8] we have presented evidence for a hitherto unnoticed relation between the total cross section $\sigma_{12}^{\text{tot}}(s)$ and slope parameter $b_{12}(s)$ for hadron-proton collisions in the diffractive energy regime, i.e., $\sqrt{s} \gtrsim 20$ GeV. For pp and $p\bar{p}$ collisions, experiment shows a quadratic relation between the total cross section and slope parameter:

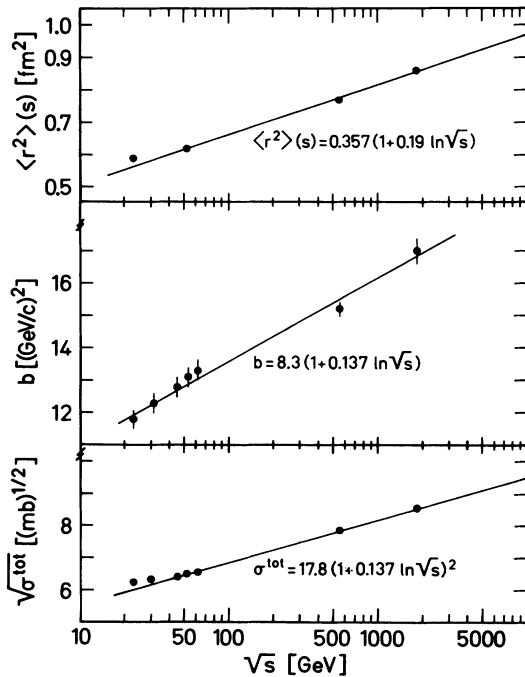


FIG. 1. Energy dependence of $\langle r^2 \rangle(s)$, the real part of the interaction radius squared, and of the total cross section and slope parameter. Note that the straight lines for $[\sigma^{\text{tot}}(s)]^{1/2}$ and $b(s)$ have the same slope.

$$\sigma^{\text{tot}}(s) = ab^2(s). \quad (2.9)$$

We have repeated the analysis of Ref. [8], including the most recent data. Figure 1 shows the slope parameter $b(s)$ and $[\sigma^{\text{tot}}(s)]^{1/2}$ for pp and $p\bar{p}$ collisions as a function of $\ln \sqrt{s}$. One observes straight lines with the *same* slopes. This analysis is the basis of our claim for Eq. (2.9). We note that Eq. (2.9) contradicts the scaling hypothesis $\sigma^{\text{tot}} \propto b$, postulated within the geometric scaling model [7]. Equation (2.9) is a constraint which any theoretical model has to reproduce and has serious consequences for existing ones (cf. Sec. IV).

C. Requirements of analyticity

We now combine the observations from Secs. II A and II B and generalize them to obtain an expression for the scattering amplitude $A(s, t)$. In order to keep the formulas transparent, we drop the index 1,2 and deal with pp and $p\bar{p}$ first. Within our geometric approach, we do not distinguish between pp and $p\bar{p}$; therefore, our amplitude $A(s, t)$ has $C=+1$. Differences between pp and $p\bar{p}$, which are seen in the total cross sections, real to imaginary parts, and interference patterns in the dip regime, are successfully accounted for by a small additional $C=-1$ contribution to the amplitude $A(s, t)$, as shown in Ref. [2].

Since the experimental slope parameter $b(s)$ depends on energy, the relation (2.6) between b and the necessarily energy-independent charge radii, which follows from the Chou-Yang conjecture, must be modified. We *define* energy-dependent hadronic radii by the equation

$$\langle r^2 \rangle(s) = \frac{3}{2}b(s). \quad (2.10)$$

Then Eq. (2.9) for the total cross section can be written in terms of the *hadronic* radii as

$$\sigma^{\text{tot}}(s) = \lambda_0 [\langle r^2 \rangle(s)]^2. \quad (2.11)$$

The radii $\langle r^2 \rangle(s)$ defined by hadronic reactions are not far in value from the electromagnetic ones [8], and this has been the reason for the Chou-Yang observation. However, the hadronic radius $\langle r^2 \rangle(s)$ does not characterize a *static* distribution of quarks and gluons in the hadron, but should be viewed as an effective *interaction* radius which increases with energy because more inelastic channels open up and new degrees of freedom of the colliding hadrons contribute.

We combine the concept of an energy-dependent radius with the shape of the t dependence of the scattering amplitude [Eq. (2.4)] by postulating the parameter Λ in the expression of the form factor $F(t)$ to be energy dependent and introduce the notation $F(t, \langle r^2 \rangle(s))$ to make the energy dependence explicit. This generalization of the t dependence of $A(s, t)$ is an economical one. One also might expect a change in the functional dependence of F as s increases. But so far there is no need for a more general shape as the comparison with the data shows (Sec. III).

At the present state of our line of arguments, the scattering amplitude is parametrized by

$$\tilde{A}(s, t) = \frac{is}{4\pi} \lambda_0 [1 - i\rho(s)] [\langle r^2 \rangle(s) F(t, \langle r^2 \rangle(s))]^2, \quad (2.12)$$

where $\rho(s)$ is the ratio of real to imaginary parts of the forward-scattering amplitude. The amplitude \tilde{A} contains the observations (2.4) and (2.9), but is not necessarily an analytic function in s . The real functions $\langle r^2 \rangle(s)$ and $\rho(s)$ are defined only for real (physical) values of s since they are taken from experiment. In order to obtain an analytical continuation, Eq. (2.12) has to be suitably modified. We have, for $t=0$,

$$\tilde{A}(s, 0) = \frac{is}{4\pi} \lambda_0 [1 - i\rho(s)] [\langle r^2 \rangle(s)]^2. \quad (2.13)$$

Analyticity of $\tilde{A}(s, 0)$ in s requires the quantity

$$R^4(s) = [1 - i\rho(s)] \langle r^2 \rangle(s)^2 \quad (2.14)$$

to be an analytic function. We call $R(s)$ the complex radius function of the hadron. If we require $A(s, t)$ to be analytical in s , we have to modify expression (2.13) to

$$\tilde{\tilde{A}}(s, t) = \frac{is}{4\pi} \lambda_0 [R^2(s) F(t, R^2(s))]^2. \quad (2.15)$$

In going from Eqs. (2.12) to (2.15), we have introduced the complex radii also into the form factors in order to guarantee analyticity in s also for $t \neq 0$. Complex radii in the form factors are not new, but have already been used in the geometric scaling model [7]. They imply that the ratio of real to imaginary parts of $\tilde{\tilde{A}}(s, t)$ depends on the momentum transfer t .

The form of the amplitude $\tilde{\tilde{A}}(s, t)$ fails to describe the differential cross section at values $|t| \gtrsim 1$ (GeV/c)². In this regime a dip and a second maximum (or a shoulder) appear and are reminiscent of double scattering in the language of multiple scattering. Whether these phenomena originate indeed from an iteration of the amplitude $\tilde{\tilde{A}}$ or if more complicated physics, such as the exchange of more Pomerons or gluons, is responsible for it does not seem to be settled. In our approach we eikonalize the scattering amplitude A by demanding that the "Born amplitude" $\tilde{\tilde{A}}(s, t)$ [Eq. (2.15)] determine the phase-shift function $\chi(s, b)$ as a function of the impact parameter b by

$$\chi(s, b) = \frac{1}{is} \int \frac{d^2q}{2\pi} e^{iq \cdot b} \tilde{\tilde{A}}(s, -q^2). \quad (2.16)$$

Then our final expression for the scattering amplitude, eikonalized and analytic in s , reads

$$A(s, -q^2) = \frac{is}{2\pi} \int d^2b e^{-iq \cdot b} (1 - e^{-\chi(s, b)}) \quad (2.17)$$

and will be confronted with experiment in Sec. III. The generalization for unequal particles is obtained by a straightforward generalization:

$$\tilde{\tilde{A}}_{12}(s, t) = \frac{is}{4\pi} \lambda_0 \prod_{i=1}^2 [R_i^2(s) F_i(t, R_i^2(s))], \quad (2.18)$$

where

$$R_i^2(s) = \frac{3}{2} b_{ii}(s) [1 - i\rho_{ii}(s)]^{1/2}. \quad (2.19)$$

III. COMPARISON WITH EXPERIMENT

Let us compare the results of the geometric model as presented above with experiment. The scattering amplitude $A_{12}(s, t)$ is calculated from Eq. (2.17) from the phase-shift function $\chi_{12}(s, b)$, for which our approach gives the parametrization

$$\chi_{12}(s, b) = \frac{\lambda_0}{4\pi} \int \frac{d^2q}{2\pi} e^{iq \cdot b} \prod_{i=1}^2 [R_i^2(s) F_i(-q^2, R_i^2(s))]. \quad (3.1)$$

We choose

$$F_i(-q^2, R_i^2) = \left[1 + \frac{q^2 R_i^2}{6n_i} \right]^{-n_i} \quad (3.2)$$

to be dipole ($n=2$) form factors for the baryons and monopole ($n=1$) ones for the mesons. The integrals (4.1) can be evaluated in terms of the modified Bessel functions $K_n(z)$. For instance, for pp or $p\bar{p}$ scattering, we obtain

$$\chi_{pp}(s, b) = \frac{\lambda_0}{16\pi} R_p^2(s) \left[\frac{\sqrt{12}b}{R_p(s)} \right]^3 K_3 \left[\frac{\sqrt{12}b}{R_p(s)} \right]. \quad (3.3)$$

The scattering amplitude is then calculated by numerical integration. There are the several free parameters in our approach.

(1) The overall strength λ_0 , a real number of dimension GeV², which is taken to be independent of the type of reaction (pp , $p\bar{p}$, πp , or Kp) and independent of the energy s .

(2) The radii $R_i(s)$ for the projectile and target particles. The $R_i(s)$ are complex functions of the energy. Therefore there are two free parameters at each energy s .

We now explain how these parameters are determined from experiment. We start with the pp data from the ISR [10] and choose data at $\sqrt{s} = 23.4$ and 53 GeV as representative experimental results. The parameters λ_0 and the real and imaginary parts of the radius $R(s)$ at this energy are fitted so as to reproduce well the data at 23.4 GeV. The region around the first minimum is found to be particularly sensitive to $R(s)$. The position fixes essentially $\text{Re}R(s)$, while the interference pattern determines $\text{Im}R(s)$. The value $\lambda_0 = 0.52$ GeV² is obtained from a good overall fit to the data of $d\sigma/dt$. The values for the radius $R(s)$ are given in Table I.

The resulting fit for $d\sigma/dt$ is shown in Fig. 2, and in Table I we compare experimental and calculated values for σ^{tot} , the slope parameter b , and ρ , the real to imaginary parts of the forward-scattering amplitude. The differential cross section is well reproduced, including the maximum after the diffraction peak, but agreement worsens for $|t| > 2$ GeV/c. Other approaches do better in this region, however, at the expense of further adjustable parameters. In the Pomeron approach, two Pomeron and $C = -1$ amplitudes are introduced, while geometric ap-

TABLE I. Summary of the input data for each reaction (real and imaginary parts of the interaction radius) and a comparison between experimental and calculated values for the total cross section, slope parameter, and ρ .

Reaction	c.m. energy \sqrt{s} (GeV)	Radius $R(s)$		σ^{tot} (mb)		b [(GeV/c) 2]		ρ		Reference
		Re R (fm)	Im R /Re R	Expt.	Calc.	Expt.	Calc.	Expt.	Calc.	
pp	23.5	0.77	0.005	38.94 ± 0.17	38	11.8 ± 0.3	11.6	0.02 ± 0.005	0.02	Amaldi <i>et al.</i> [10]
	52.8	0.79	0.01	42.67 ± 0.19	41	13.1 ± 0.3	12.2	0.078 ± 0.01	0.046	
$p\bar{p}$	546	0.88	0.04	61.9 ± 1.5	60	15.2 ± 0.2	15.4	0.24 ± 0.04	0.14	Bozzo <i>et al.</i> [11]
	1800	0.93	0.04	73.3 ± 3.0	73	17.02 ± 0.46	17.6	0.126 ± 0.067	0.14	Amos <i>et al.</i> [12]
$p\bar{p}$	16 000	1.01	0.04		95		21		0.14	prediction
	40 000	1.04	0.04		107		23		0.14	
π^+p	20	0.64	0	23.78 ± 0.04	24	9.25 ± 0.12	9.8	0.04		Akerlof <i>et al.</i> [13]
K^+p	20		0	19.91 ± 0.11	20	8.13 ± 0.37	9			

proaches use a t -dependent interaction function in addition to the t dependence in the form factors. We prefer to stay with the discrepancy at large t .

Among all the data from the ISR, the data for $d\sigma/dt$ at 53 GeV are the most difficult to describe (Fig. 3). We have chosen these data nevertheless in order to show also a bad fit. The freedom in adjusting the real and imaginary parts of the radius is not too large. The imaginary part of the radius has here a value 1% of Re R . This small value of Im R suffices to account for the shape of the dip in $d\sigma/dt$ and for a rough agreement with the experimental value of ρ (Table I). It also introduces a rather complicated pattern into the t dependence of Re $A(s,t)$. Figure 4 shows the behavior of Re $A(s,t)$ and Im $A(s,t)$ for $\sqrt{s}=53$ GeV as a function of t . The scattering amplitude $A(s,t)$ is basically imaginary. Im $A(s,t)$ shows a zero in the region of the first minimum [$t \simeq 1.2$ (GeV/c) 2]. The real part is not constant as a function of t , but has a zero for $t \simeq 0.3$ (GeV/c) 2 . Therefore the relation between the phase of the amplitude at the minimum, which we use to determine Im $R(s)$, and the phase at $t=0$, where ρ is measured, is rather complicated.

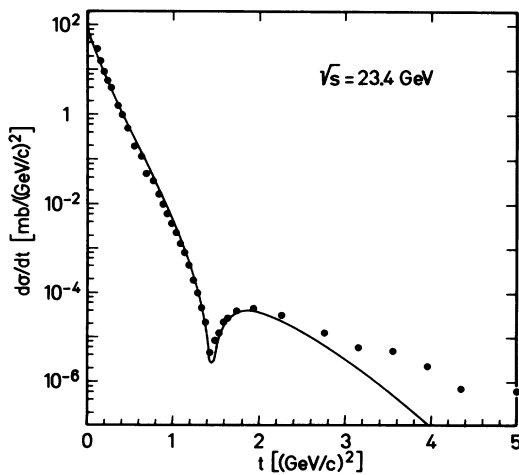


FIG. 2. Differential elastic cross section for pp scattering at $\sqrt{s}=23.4$ GeV. The data (of which only a part are shown) are from the ISR experiment [10]. The solid curve is our fit as described in the text and with parameters given in Table I.

We pass to the data for $p\bar{p}$ at 546 GeV [11]. The differential cross section is shown in Fig. 5. There has been an extensive discussion on the large experimental value for the ratio ρ of the real to imaginary parts of the forward amplitude. We show fits to the data for three choices for the imaginary part of the radius. The situation in the middle [Fig. 5(b)] is our best fit and corresponds to a value $\rho=0.14$. The calculation shown in Fig. 5(a) predicts $\rho=0.07$, and $\rho=0.21$ relates to Fig. 5(c). The latter value would be close to the experiment, but the fit to the data [Fig. 5(c)] seems unacceptable. We note that our best value $\rho=0.14$ for $\sqrt{s}=546$ GeV relates to the experimental result $\rho=0.126 \pm 0.067$ for $\sqrt{s}=1.8$ TeV, although the error bars are still rather large. The fit to the data [12] at 1.8 TeV is shown in Fig. 6. Since the data do not include the first minimum, we are not able to determine Im R at this energy. We take it the same as for the best fit at 546 GeV.

Before we proceed to predictions at even higher energies, we remind the reader of the systematics of the fitted values for the radius constant $\langle r^2 \rangle(s) \equiv R^2(s)$ as shown in Fig. 1. The real parts of the values $R^2(s)$, which are obtained by fitting the data, especially the dip

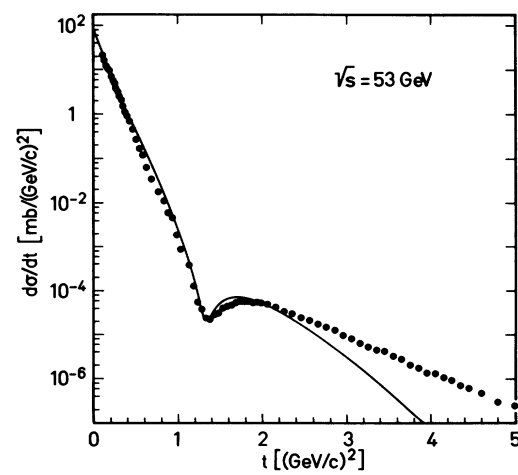


FIG. 3. Differential elastic cross section for pp scattering at $\sqrt{s}=53$ GeV. The data (of which only a part are shown) are from the ISR experiment [10]. The solid curve is our fit as described in the text and with parameters given in Table I.

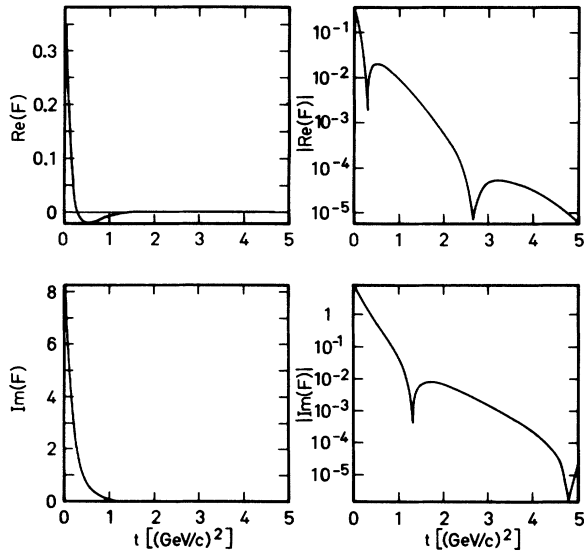


FIG. 4. t dependence of $\text{Re}A(s,t)$ and $\text{Im}(s,t)$ for $\sqrt{s} = 53$ GeV plotted linearly and logarithmically.

region at each energy, are drawn as a function of $\ln\sqrt{s}$ and show a linear dependence. The value at 23.4 GeV is still a little above the systematics, which may be explained by contributions from meson exchange which have not completely died out [8]. The energy dependence of the radius, as seen in Fig. 1, can be written as

$$\text{Re}R^2(s) = (0.60 \text{ fm})^2 (1 + 0.19 \ln\sqrt{s}). \quad (3.4)$$

The observation from Fig. 1, that the slope parameter and total cross section increase slightly slower with energy than the radius $\text{Re}R(s)$, stems from the fact that the eikonalization of the amplitude slightly changes the relation between $R^2(s)$ and σ^{tot} from those in the Born approximation.

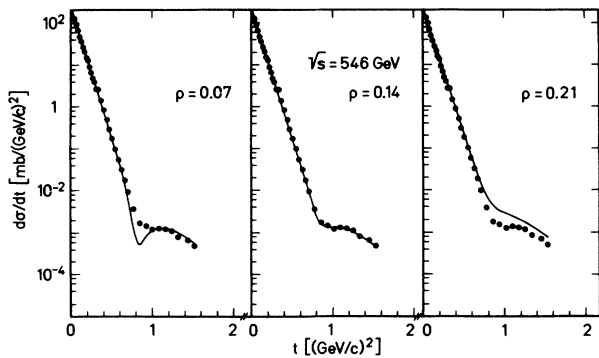


FIG. 5. Differential elastic cross section for $p\bar{p}$ scattering at the SPS accelerator at $\sqrt{s} = 546$ GeV [10]. We show three fits to the data, which differ in the imaginary part of the interaction radius R . From these values one calculates a ratio ρ of real to imaginary parts of the forward amplitude $\rho = 0.07$ (left), $\rho = 0.14$ (middle), and $\rho = 0.21$ (right).

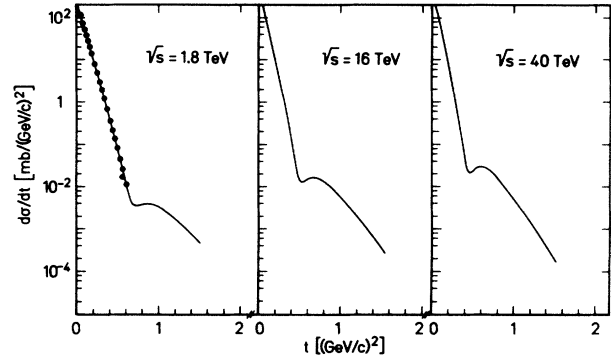


FIG. 6. Differential elastic cross section for $p\bar{p}$ at 1.8 TeV (data from Fermilab [12] and our fit) and predictions for $\sqrt{s} = 16$ and 40 TeV.

Furthermore, the systematics for the energy dependence of the radius (Fig. 1) can be used for a rather safe extrapolation to higher energies. We show our predictions for $\sqrt{s} = 16$ and 40 TeV in Fig. 6, in addition to that for $\sqrt{s} = 1.8$ TeV. Table I contains the corresponding values for the total cross sections and slope parameters. The values $\rho(s)$ of the real to imaginary parts of the forward-scattering amplitude seem to reach the constant value 0.14 for $\sqrt{s} = 500$ GeV and above. This value is in good agreement with $\rho(s) = \pi\epsilon/2 = 0.12$ (cf. Sec. IV).

Finally, Figs. 7 and 8 show the differential cross sections [13] for π^+p and K^+p scattering and Table I the corresponding slope parameters and total cross sections for $\sqrt{s} = 20$ GeV. The overall strength λ_0 and complex proton radius at this energy are known from the pp experiment at 23 GeV; only the radius constants for the pion and kaon have to be inserted. We take them to be equal to the charge radii and give their values in Table I. The differential cross sections as well as the values for σ^{tot} and b are parameter-free predictions and agree fairly well with experiment.

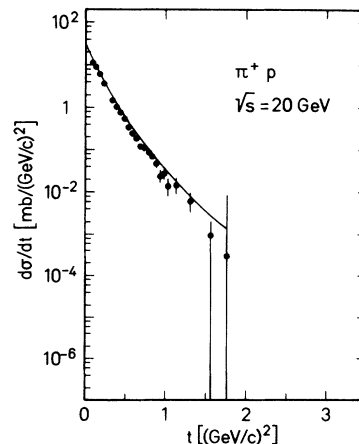


FIG. 7. Differential cross sections for πp collisions at $\sqrt{s} = 20$ GeV. The data are from Ref. [13].

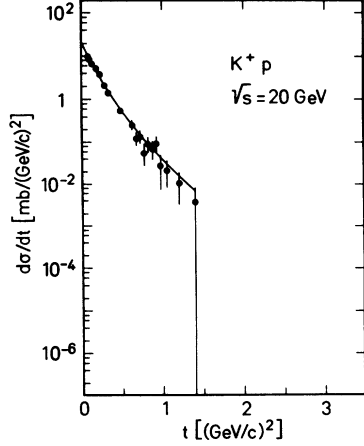


FIG. 8. Differential cross sections for Kp collisions at $\sqrt{s} = 20$ GeV. The data are from Ref. [13].

IV. COMPARISON WITH THE POMERON PARAMETRIZATION

Regge theory applied to high-energy collisions, where $\sigma^{\text{tot}}(s)$ is constant or slowly rising, has led to postulate a new trajectory, the Pomeron trajectory $\alpha(t)$, with an intercept $\alpha(0)$ close to 1. In recent years Donnachie and Landshoff [2] have extensively applied this theory to the data. The amplitude for one-Pomeron exchange is parametrized as

$$A_P(s, t) = -\lambda_P e^{-i\pi\alpha(t)/2} \left[\frac{s}{s_0} \right]^{\alpha(t)} F_1^2(t), \quad (4.1)$$

where λ_P is independent of the variables s and t and $F_1(t)$ is the Dirac electromagnetic form factor, which differs from the expressions [Eq. (2.7)] by a factor $(4m^2 - 2.79t)/(4m^2 - t)$ for the proton and takes account of the anomalous magnetic moment. $F_1(t)$ does not contain a complex energy-dependent effective radius. The authors of Ref. [2] use $\sqrt{s_0} = 2$ GeV and parametrize

$$\alpha(t) = 1 + \epsilon + \alpha'(0)t, \quad (4.2)$$

where ϵ , $\alpha'(0)$, and the overall strength λ_P are fit parameters. We compare the scattering amplitudes $A(s, t)$ in the geometric parametrization [which we denote $A_G(s, t)$] and in the Pomeron parametrization [denoted by $A_P(s, t)$] for small values of t in which the form factors can be approximated by exponentials in t . For this domain in t , the eikonalization of the geometric amplitude is not very important and we may restrict ourselves to the Born amplitude, which reads in the approximation of exponential form factors

$$A_G(s, t) = is \lambda_G R^4(s) \exp \left[\frac{t}{3} R^2(s) \right]. \quad (4.3)$$

Also, with exponential form factors, the Pomeron amplitude is

$$A_P(s, t) = is \frac{\lambda_P}{s_0} \exp \left[-i \frac{\pi}{2} [\alpha(t) - 1] \right] \left[\frac{s}{s_0} \right]^{\alpha(t) - 1} \times \exp \left[\frac{t}{3} \langle r_1^2 \rangle \right]. \quad (4.4)$$

The data suggest a logarithmic growth of the radius $R^2(s)$ with energy,

$$R^2(s) = \langle r^2 \rangle (s_1) (1 + c \ln s/s_1) [1 - i\rho(s)]^{1/2}, \quad (4.5)$$

and a phase factor related to $\rho(s)$. The mean-squared radius $\langle r_1^2 \rangle$ of the Dirac form factor $F_1(t)$ is

$$\langle r_1^2 \rangle = \langle r_{\text{ch}}^2 \rangle - \frac{2.78}{m^2}, \quad (4.6)$$

in the expression for the Pomeron amplitude. In the geometric approach, the free parameters are λ_G , c , s_1 , $\langle r^2 \rangle (s_1)$, and the function $\rho(s)$. On the other hand, the constants λ_P , ϵ , and $\alpha'(0)$ are undetermined in the Pomeron picture. We relate the parameters of the two approaches by requiring that both amplitudes [Eqs. (3.3) and (3.4)] describe the same physics, i.e., are just two different parametrizations of the same amplitude. The dimensionless parameters $|\epsilon|$, $|c \ln s/s_1|$, and $|\rho(s)|$ turn out to be small compared with 1. We have no prescription for the choice of s_1 and therefore choose it for calculational convenience as $\sqrt{s_1} = 200$ GeV, which is the logarithmic middle point of the interval (20 GeV, 2 TeV). Working to first order in these quantities, one arrives after some algebra at

$$c = \epsilon/2, \quad (4.7)$$

$$\rho(s) = \frac{\pi}{2} \epsilon, \quad (4.8)$$

$$\alpha'(0) = \frac{\langle r_1^2 \rangle (s_1)}{6} \epsilon. \quad (4.9)$$

With the help of these relations, the complex energy-dependent radius $R(s)$ and the Pomeron trajectory $\alpha(t)$ can be written in terms of only two parameters ϵ and $\langle r^2 \rangle (s_1)$:

$$R^2(s) = \langle r^2 \rangle (s_1) \left[1 + \frac{\epsilon}{2} \left[\ln s/s_1 - i \frac{\pi}{2} \right] \right], \quad (4.10)$$

$$\alpha(t) = 1 + \epsilon \left[1 + \frac{\langle r^2 \rangle (s_1)}{6} t \right]. \quad (4.11)$$

The relations (4.10) and (4.11) are the central results of this section. We want to discuss the relation [Eq. (4.11)] between $\epsilon = \alpha(0) - 1$ and the slope $\alpha'(0)$. First, a comparison with “experiment”: In Ref. [2], ϵ and $\alpha'(0)$ have been determined independently from the data to $\epsilon = 0.08$ and $\alpha'(0) = 0.25$ (GeV/c) $^{-2}$. Using $\langle r^2 \rangle (s_1) = 0.72$ fm 2 from Fig. 1, we find, from Eq. (4.11),

$$\alpha'(0) = 0.24$$
 (GeV/c) $^{-2}$, (4.12)

in good agreement with the experimental value. Relation (4.11) between the intercept $\epsilon = \alpha(0) - 1$, the slope $\alpha'(0)$ of the Pomeron trajectory, and the mean-squared radius

of the colliding nucleons is unexpected, since the properties of the exchanged trajectories are not necessarily related to properties of the colliding hadrons. Since relation (4.11) has generated some controversy, we want to give another derivation for Eq. (4.11) which does not relate to the geometric model, but only uses the expression for the Pomeron amplitude [Eq. (4.4)] together with the experimental relation $\sigma^{\text{tot}}(s) = \text{const} \times b^2(s)$ between the total cross section and slope parameter $b(s)$. One derives, from the Pomeron amplitude [Eq. (4.4)] to first order in $\epsilon \ln s/s_1$,

$$\sigma^{\text{tot}}(s) = \frac{4\pi\lambda_P}{s_0} \left(\frac{s_1}{s_0} \right)^\epsilon (1 + \epsilon \ln s/s_1), \quad (4.13)$$

$$b(s) = \frac{2}{3} \langle r_1^2 \rangle \left[1 + \frac{3\alpha'(0)}{\langle r_1^2 \rangle} \ln s/s_0 \right]. \quad (4.14)$$

The energy dependence of the total cross section is governed by the intercept $\epsilon = \alpha(0) - 1$, while the rise of the slope parameter $b(s)$ with energy is determined by $\alpha'(0)$. Any relation between the total cross section and slope parameter imposes a relation between α' and ϵ . Empirically (see Fig. 1), the energy dependences of $(\sigma^{\text{tot}})^{1/2}$ and $b(s)$ are the same within the interval considered; therefore,

$$\frac{1}{2}\epsilon = \frac{3\alpha'(0)}{\langle r_1^2 \rangle \ln s_1/s_0}, \quad (4.15)$$

where $\langle r_1^2 \rangle \ln s_1/s_0 \approx \langle r^2 \rangle (s_1)$. This derivation makes clear that Eq. (4.15) or, equivalently, Eq. (4.9) is imposed by experiment, once one uses the one-Pomeron-exchange amplitude to describe elastic-scattering properties at low t . We come back to Eqs. (4.10) and (4.11), which express the central quantities, the effective radius $R^2(s)$ in the geometrical approach and the Pomeron trajectory $\alpha(t)$ in the Regge description, in terms of only two parameters $\langle r^2 \rangle (s_1)$ and ϵ . It is remarkable that both $R^2(s)$ and $\alpha(t)$ depend on the *same* two quantities, although they are very different mathematically and physically. α is a function of t , while R^2 is a function of s . α describes a trajectory, i.e. a series of Regge poles or particles, while R^2 is

an effective interaction radius. The same small quantity ϵ determines the intercept $\alpha(0) - 1$ and slope parameter $\alpha'(0)$, as well as the logarithmic energy dependence of the radius $R^2(s)$. The dependence of $R^2(s)$ and $\alpha(t)$ on the same parameters points to a common origin of the two pictures, the geometric and Regge pole ones. However, we are unable to clarify this common origin.

V. SUMMARY

We have presented a phenomenological approach to the elastic scattering of hadrons in the diffractive energy regime $\sqrt{s} \gtrsim 20$ GeV. The basic idea is a geometric one: The differential and total cross sections are determined by the shape of the colliding hadrons. The more refined analysis, presented in this paper, indicates that the "interaction form factor" of the hadrons varies with energy whose variation can be accounted for by an energy-dependent radius. For reasons of analyticity, the radius has to be complex. While the energy dependence of the radius indicates that this is an effective *interaction* radius, the physical interpretation of its imaginary part is unclear to us. The real part of the radius increases linearly with $\ln s$, which makes predictions to higher energies rather straightforward.

Our parametrization of the scattering amplitude in terms of the radius gives a good fit to the data of $d\sigma/dt$ up to $t \approx 2$ (GeV/c)², but fails at higher values of t . The transition from pp to πp and Kp is straightforward, since only the radii for the projectile have to be changed, but not the overall strength. We think that the presented model is a very economical model in that it contains few parameters only, most of which have direct physical interpretation.

ACKNOWLEDGMENTS

We gratefully acknowledge discussions with O. Nachtmann and A. Schäfer. We thank A. Donnachie and P. Landshoff for their comments relating to Sec. IV in particular. This work has been partly supported by the Bundesminister für Forschung und Technologie under Contract No. 06 HD710.

-
- [1] L. L. Jenkovszky, Fortschr. Phys. **34**, 791 (1986); M. Block and R. Cahn, Rev. Mod. Phys. **57**, 563 (1985).
 - [2] A. Donnachie and P. V. Landshoff, Nucl. Phys. **B231**, 189 (1984); **B244**, 322 (1984); **B267**, 690 (1986); **B311**, 509 (1989).
 - [3] F. E. Low, Phys. Rev. D **12**, 163 (1975); S. Nussinov, Phys. Rev. Lett. **34**, 1286 (1975).
 - [4] P. V. Landshoff and O. Nachtmann, Z. Phys. C **35**, 405 (1987); O. Nachtmann, Ann. Phys. (N.Y.) **209**, 436 (1991).
 - [5] T. T. Chou and C. N. Yang, Phys. Rev. **170**, 1591 (1968); Phys. Rev. D **19**, 3268 (1979); Phys. Lett. **128B**, 457 (1983); Phys. Lett. **B 244**, 113 (1990).
 - [6] C. Bourrely, J. Soffer, and T. T. Wu, Nucl. Phys. **B247**, 15 (1984); Phys. Rev. Lett. **54**, 757 (1985); Phys. Lett. **B 196**, 237 (1987).
 - [7] J. Dias de Deus and P. Kroll, Nuovo Cimento A **37**, 67 (1977); Acta Phys. Pol. B **9**, 157 (1978); P. Kroll, Z. Phys. **C 15**, 67 (1982).
 - [8] B. Povh and J. Hüfner, Phys. Rev. Lett. **58**, 1612 (1987); Phys. Lett. **B 215**, 772 (1988).
 - [9] R. J. M. Covelan, L. L. Jenkovsky, and E. Predazzi, Z. Phys. C **51**, 459 (1991).
 - [10] A. Böhm *et al.*, Phys. Lett. **49B**, 491 (1974); E. Nagy *et al.*, Nucl. Phys. **B150**, 221 (1979); A. Breakstone *et al.*, *ibid.* **B248**, 253 (1984); U. Amaldi *et al.*, Phys. Lett. **53B**, 231 (1973); **62B**, 460 (1976); U. Amaldi and K. R. Schubert, Nucl. Phys. **B166**, 301 (1980); N. Amos *et al.*, Phys. Lett. **120B**, 460 (1983).
 - [11] M. Bozzo *et al.*, Phys. Lett. **147B**, 385 (1984); **147B**, 394 (1984); UA4 Collaboration, D. Bernard *et al.*, Phys. Lett. **B 198**, 583 (1987).
 - [12] N. A. Amos *et al.*, Phys. Lett. **B 243**, 158 (1990); Phys. Rev. Lett. **63**, 2784 (1989); S. Shekar (private communication).
 - [13] C. W. Akerlof *et al.*, Phys. Rev. D **14**, 2864 (1976); A. S. Carrol *et al.*, Phys. Lett. **80B**, 423 (1979).